1   **Fill dynamics and sample mixing in the AirCore**

2   **Pieter P. Tans**

3   **Global Monitoring Laboratory, National Oceanic and Atmospheric Administration**

4   **325 Broadway, Boulder, CO 80305**

6   **Abstract**

7   The AirCore is a long coiled tube that acts as a "tape recorder" of the composition of air as it is
8   slowly filled or flushed. When launched by balloon with one end of the tube open and the other
9   closed, the initial fill air flows out during ascent as the outside air pressure drops. During descent
10   atmospheric air flows back in. I describe how we can associate the position of an air parcel in the
11   tube with the altitude it came from by modeling the dynamics of the fill process. The conditions
12   that need to be satisfied for the model to be accurate are derived. The extent of mixing of air
13   parcels that enter at different times is calculated, so that we know how many independent
14   samples are in the tube upon landing, and later when the AirCore is analyzed.

16   **1. Introduction**

17   When the Aircore is filling with atmospheric air coming in through the open end the newly
18   sampled air pushes the air that is already in the tube deeper into the tube while compressing it.
19   This mode of sampling is entirely passive, relying on the pressure continuing to increase as the
20   altitude becomes lower during descent. The AirCore could also be flushed by a pump without
21   any need for pressure changes of the outside air that is being sampled. I conceived the idea of
22   AirCore in the late 1990s after we had found ~100 year old air, as indicated by the measured
23   levels of CO_2 and CH_4, near the bottom of the firn layer at a depth of ~90 m at the South Pole
24   (Battle, 1996). The air was very old despite the fact that there was still open contact with the
25   present-day atmosphere. Over distances of tens of meters or more molecular diffusion is
26   exceedingly slow! The root-mean-square (rms) molecular diffusion distance is $X_{rms}= (2Dt)^{0.5}$. D
27   is diffusivity in air, for CO_2 it is 0.140 cm^2 s^{-1} at 1 bar and 0 degree C, t is time in seconds. After
28   one year the rms diffusion distance for CO_2 in air would be ~30 m which would be the scale of
29   spreading if there is no macroscopic air motion at all. In addition, diffusive mixing deep in the
30   firn is significantly slower than in open air because the air path from the bottom of the firn to the
31   atmosphere has many detours going through the pores that are still open.

32   With Jim Smith and Michael Hahn, two members of our group in those days, we verified that
33   there is very little mixing along the length of the tube by pushing slugs of air from two different
34   reference air cylinders, alternating between high and low CO_2, through a long coiled tube. We

35   also stored air for several hours before analysis. It all looked good. Then we tried a balloon
36   flight. In order to make the payload lighter we switched from stainless steel to aluminum tubing,
37   because of our excellent experience with long term gas storage in high pressure aluminum
38   cylinders. It did not work at all. The easily bendable tube was made of a soft aluminum alloy,
39   very different from the high pressure cylinders. We found that the tube consumed CO_2 very
40   effectively. It was going to take more effort to make it successful, and we did not have much
41   time to devote to it. So the project languished for several years until Anna Karion, Colm
42   Sweeney, and Tim Newberger of our group at GML were able to pick it up again. At the urging
43   of Sandy MacDonald, who was director of NOAA's Earth System Research Laboratory at the
44   time, I applied for a patent in August 2006. He pointed out that there are people trolling the
45   scientific literature, conference proceedings, etc. to find ideas that could be patented, so that we
46   might find ourselves having to pay somebody else to use our own idea. Instead, we wanted the
47   AirCore to be freely useable (and improved) by everyone, so that my patent (Tans, 2009) was
48   intended to be a defensive action!

49   We realized that AirCore technology could become extremely useful for the validation of
50   satellite retrievals of column-averaged mole fractions of greenhouse gases. The measurements of
51   a gas sample captured by the AirCore are calibrated, but care has to be taken, as with all air
52   samples in containers, that no artefacts are introduced by the container or by gas handling
53   procedures. In contrast, remote sensing estimates of greenhouse gases can in principle never be
54   calibrated. Metrology, the science of measurement, defines what a calibration is. Using a
55   measurement standard, one presents the measurement method with a known value, under
56   controlled conditions, so that the measurement indication is related to a quantity value
57   (paraphrased from VIM3, JCGM 200:2008). In the case of greenhouse gases in the atmosphere
58   the conditions cannot be controlled. In addition, we realized that the regular deployment of
59   AirCores could be a cost effective way to monitor and study an evolving atmospheric circulation
60   as climate change progresses, as proposed by Fred Moore(Moore et al., 2014).

61   Developments of the AirCore by various groups has been described in other papers, for example
62   by Wagenhäuser et al. (2021) and Membrive et al. (2017). However, there has not been a
63   comprehensive treatment of fill dynamics, nor a detailed look at mixing. Hence this paper.

64

2. The physical principle that makes the AirCore work – molecular diffusion

66   Diffusive mixing over large distances is exceedingly slow, but there is another use of diffusion.
67   Flow inside the tube is laminar, which has maximum speed in the center and zero speed at the
68   wall. With velocities that differ from zero to some finite value, why does laminar flow **not**
69   "smear out" our tape recorder signal by mixing air parcels that came in at different times? Again,
70   molecular diffusion comes to the rescue. Using the square root relationship above, if the inner
71   radius of the tube is 0.3 cm, it takes a CO_2 molecule on average only 0.03 s (at 1 bar pressure) to

72   diffuse from the wall to the radius where the velocity equals the average velocity inside the tube.
73   Any molecule will be close to the wall, as well as near the center, of the tube many times per
74   second. Therefore the speed of all molecules in the long direction of the tube, averaged over a
75   few seconds, is very nearly the same. However, the AirCore idea does not work so well for
76   liquids. In water the molecular diffusivity is ~10,000 times lower than in air at 1 bar, so that the
77   smearing of a tape recorder signal could be very large. To compensate for such low diffusivity
78   both the diameter of the tube and the flow speed will have to be kept low, and there will also be
79   capillary effects. Water may be attracted to, or repelled by, the tube wall, influencing the flow.

80   The AirCore collects a continuous sample. Instead of valves, distance in the tube is used to keep
81   separated the air that has been sampled from different pressure altitudes. The number of
82   independent samples (the inverse of vertical resolution) in the tube decreases as the time between
83   collection and measurement becomes longer. The measurement, or "read-out" of the vertical
84   profile, is carried out by attaching an analytical instrument to one end of the tube and a cylinder
85   with air of well-known composition to the other end. The latter pushes the sampled air slowly
86   through the analyzer. The procedure, as well as various tests of mixing, has been described by
87   Karion of GML (2010).

88

89   **3. Dynamics of the fill process**

90   How do we accurately associate position in the tube with the geometric altitude or pressure
91   altitude that the sample at that position came from? It is the first question we address in this
92   paper. The filling does not occur uniformly as a function of pressure altitude. The second
93   question is how far the mixing of adjacent air parcels extends as a result of molecular diffusion,
94   and secondarily as a result of the flow itself will be addressed in section 6. I wrote the first
95   version of the fill dynamics calculation to make the association of altitude with position in 2005,
96   called rocketfall.pro, coded in Interactive Data Language (IDL). Undergraduate students in the
97   engineering department at the University of Colorado were getting ready to put an AirCore on a
98   NASA rocket, and I was worried about there not being enough time to passively collect air from
99   the stratosphere as the rocket was falling at supersonic speeds. There have been several
100 successive versions of the algorithm since then. An intermediate version was translated from
101 IDL, first into Matlab by Colm Sweeney of GML in 2013, and in 2017 from Matlab into Python
102 by Jonathan Bent of GML. The significantly improved IDL version of July 2021 is described in
103 this paper.

104 We use a fluid dynamics model and a subset of flight data, namely the time, pressure and
105 temperature of outside air and the temperature of the tube as input data. The starting point is
106 Poiseuille's equation for steady state laminar flow in a tube with circular cross section:

107 $$Q_m = \frac{-\rho \, \pi \, r^4}{8 \, \eta} \frac{dP}{dz} \, , \quad \text{or} \quad Q_n = \frac{-\rho_n \, \pi \, r^4}{8 \, \eta} \frac{dP}{dz} \qquad \qquad \text{Eq. (1)}$$

108   in which Q_m is mass flow (kg s^{-1}), $Q_n = Q_m/M$ is amount flow (mol s^{-1}) with M molecular weight

109   of dry air (0.02896 kg mol^{-1}), ρ is gas density (kg m^{-3}), ρ_n is amount density (ρ/M in mol m^{-3}), η

110   is viscosity (kg m^{-1} s^{-1}), r is tube radius (m), P is pressure in Pascal (kg m^{-1} s^{-2}), and z is

111   distance along the tube (m). Pressure is given by the ideal gas law as $P = (n/V)\,RT$, with $n/V = \rho_n$

112   the number density in mol m^{-3}, T is temperature in degrees Kelvin (K), and R the universal gas

113   constant, 8.3144 J mol^{-1} K^{-1}. The flow velocity is parabolic as a function of radius, zero at the

114   wall, and maximum in the center where the speed is twice the average speed.

115   The viscosity (η) depends on temperature, but it is very nearly independent of pressure in our

116   range of interest. The latter is of primary importance to the fill process. A simple approximate

117   molecular expression for viscosity is $\eta \cong (1/3)\,\rho\,\mathbf{c}\,\lambda$, in which $\mathbf{c}$ is the average molecular speed

118   and λ is the mean free path between collisions which is inversely proportional to ρ (Jeans, 1952)

119   so that it cancels the factor "ρ" in $(1/3)\,\rho\,\mathbf{c}\,\lambda$. Since the volume flow (m^3 s^{-1}) is $Q_v = Q_m/\rho$, Eq.

120   (1) states that the volume flow depends on viscosity, but not on gas density. It takes the same

121   amount of force (pressure difference) to push a volume flow irrespective of the density of air in

122   that volume. During steady flow through any tube the flow needs to speed up at the low pressure

123   end to conserve mass, so that the pressure gradient always steepens at the low pressure end.

124   The z-coordinate is for position along the length of the tube. The pressure change at any point in

125   a small section of the tube with length dz can be due to temperature change or to more amount

126   flow coming in from z than leaving from z+dz. The latter term is

127
$$\frac{d\rho_n}{dt} = -\frac{1}{\pi r^2}\frac{dQ_n}{dz}\,, \quad \text{so that}$$

128
$$\frac{dP}{dt} = \rho_n R\frac{dT}{dt} + RT\frac{d\rho_n}{dt} = \frac{P}{T}\frac{dT}{dt} - \frac{RT}{\pi r^2}\frac{dQ_n}{dz} \qquad \text{Eq. (2)}$$

129   Because we assumed that the tube cross section is round (not elliptical for example) the amount

130   flow Q_n is given by Poiseuille's equation, and Eq. (2) can be represented numerically in a very

131   efficient manner. In that case the flow is in effect solved as a succession of steady state flows

132   that evolve slowly in time and along the length of the tube. In the rest of this section we will

133   discuss a number of assumptions we are making for our "succession of steady state flows"

134   approximation to Eq. (2) to be satisfactory.

135   The first one is that inertial effects, i.e. accelerations, die out very rapidly. Suppose we suddenly

136   set the pressure gradient that is driving the flow to zero. What is the time scale for the flow to die

137   down? We can estimate the time it takes for the flow to adjust by using Eq. (1). The average

138   speed of the flow is $\mathbf{v}_{avg} = Q_v/(\pi r^2) = (r^2/8\eta)\,(\Delta P/\Delta z)$. The momentum of the flow in length Δz is

139    $\mathbf{v}_{avg}\,\rho\,\pi\,r^2\,\Delta z$ which equals $Q_m\Delta z$ (neglecting the sign). The rate of change of momentum is

140   given by the frictional force which is equal and opposite to the pressure force that was driving

141   the flow in Eq. (1). The adjustment time scale of the flow is momentum divided by the frictional

142   force,

143
$$\tau = \frac{Q_m \, \Delta z}{\Delta P \, \pi r^2} = \frac{\rho \, r^2}{8 \, \eta}$$
Eq. (3)

144 For a tube with a radius of 3 mm and ρ corresponding to 1 bar and 285 K, $\tau \cong 0.07$ s. At an
145 altitude where the density is 10 times lower (~18 km), $\tau \cong 0.007$ s. Recently NOAA GML has
146 been flying AirCores with $r \cong 1.46$ mm, for which the adjustment time at 1 bar and 285 K is $\tau \cong$
147 0.017 s. A succession of steady state flows is indeed a very close approximation.

148 Next we assume that the temperature of the gas is the same as that of the wall. How rapidly does
149 the temperature of the gas equilibrate with the wall of the tube? The heat capacity of a volume of
150 air is $c_p \, \rho_n \cong (7/2)$ R * P/RT in which c_p is the molar heat capacity at constant pressure and ρ_n is
151 the number density (mol m^{-3}) of the gas, so that $c_p \, \rho_n$ has units of J m^{-3} K^{-1}. The heat
152 conductivity of gas is $\kappa \cong (1/3) \, c_v \, \rho_n \, \mathbf{c} \, \lambda$ (Jeans, 1952) in which c_v is the molar heat capacity at
153 constant volume, $\mathbf{c}$ is the average speed of individual molecules and λ the mean free path. It has
154 units of (J/s) m^{-2} (K/m)$^{-1}$, the heat flow per area per temperature gradient. As in the previous
155 paragraph we divide the heat energy change corresponding to ΔT in a volume of gas residing in a
156 length Δz by the heat flow from the wall assuming the temperature gradient is close to
157 $(\Delta T/(0.5r)$. That gives

158
$$\tau = \frac{c_p \rho_n \, \pi r^2 \Delta z \, \Delta T}{(1/3) \, c_v \rho_n \, \mathbf{c} \, \lambda \, 2\pi \, r \, \Delta z \, \Delta T/(0.5r)} = \frac{c_p}{c_v} \frac{3 \, r^2}{4 \, \mathbf{c} \, \lambda}$$
Eq. (4)

159 which has units of seconds. For r = 3 mm and λ corresponding to 1 bar, and 285 K, the
160 adjustment time is $\tau \cong 0.31$ s, and shorter at lower pressures. For r = 1.46 mm $\tau \cong 0.07$ s.

161 Is the flow always laminar as Eq. 1 assumes? If Reynolds number, Re = $(\rho \mathbf{v}_{avg} d)/\eta$, in which d is
162 the diameter of the tube, stays below 1000, the flow will remain laminar. Re is estimated from
163 the calculated velocities, ρ/η, and tube dimensions for every flight. It is highest just before
164 landing when it typically has a value of ~15.

165 The tube is wound up in a coil with typical diameter 20 to 30 cm. As the flow goes around the
166 coil there will be a centrifugal force away from the center of the coil. The centrifugal force is
167 greatest where the flow has the maximum velocity, 2 $\mathbf{v}_{avg}$, very near the center of the tube. This
168 sets up a secondary flow in the plane perpendicular to the main flow, outward in the center of the
169 tube and back along the walls. The location of maximum velocity is also pushed outward a bit.
170 This increases flow resistance leading to slightly lower Q_m for the same pressure gradient in the
171 dimension z along the length of the tube. However, there are other subtle effects with the
172 opposite sign that could facilitate the flow a little (Berg, 2005). Correction factors to flow in a
173 straight tube have been calculated using Dean's number, De = Re $(r/R)^{0.5}$, in which Re is
174 Reynolds number and R is the coil radius. NOAA GML has flown AirCores with r/R from 1/50
175 to 1/70. Thus De is always smaller than 15 $(0.02)^{0.5} \cong 2$ during a flight. Berg et al. (2005)
176 present data to estimate that the relative flow correction is smaller than +1 10^{-5} for our

177   parameters. If we were to wind our coil much tighter, say with r/R of 1/20, then the maximum

178   relative flow correction during a flight would be $+2 \cdot 10^{-4}$ for the same Reynolds number.

179   Therefore we can neglect the corrections for the tube coil curvature.

180   If the tube cross section is elliptical (as a result of bending, for example) instead of circular, we

181   can use a good approximation for the change in flow resistance. Following Lekner (2019), Eq.1

182   can be written for volume flow as $(\eta \, Q_v) / (dP/dz) = \pi \, r^4 / 8$, neglecting the sign. Note that $\pi \, r^4 /$

183   8 equals $A^3 / (2 \, P^2)$ for a circular cross section, with A the cross sectional area, and P the

184   perimeter of the tube. Lekner shows that $A^3 / (2 \, P^2)$ applies quite generally for many cross

185   sectional shapes. So if the tube is somewhat squashed into an ellipse with major axis 1.05 times

186   the original radius, and a minor axis slightly smaller (in order to keep the perimeter the same)

187   than 0.95 times radius, the term $A^3 / (2 \, P^2)$ has become ~1% smaller. This correction is not

188   major, but easy to apply if needed.

189   We assumed the ideal gas law. Non-ideality is often described by the virial expansion relating

190   pressure and density, $PV/nRT = 1 + B(n/V) + C(n/V)^2 + \ldots$ Note that n/V is called ρ_n above.

191   Taking only the second (and largest) virial coefficient B (m^3 mol^{-1}) into account we can

192   approximate the number density ρ_n as (P/RT)(1-BP/RT). The relative change of number density

193   is thus BP/RT which has dimension one. At 300 K and 1 bar, B is $-7.3 \cdot 10^{-6}$ m^3/mol

194   (Sevast'yanov, 1986) which leads to a relative density increase of $2.9 \cdot 10^{-4}$. B increases to -18.9

195   10^{-6} and $-37.8 \cdot 10^{-6}$ m^3 mol^{-1} at 250 K and 200 K respectively, but at the higher altitudes the

196   density is lower so that the largest non-ideality effect occurs near the ground. Therefore the

197   fractional density increase relative to ideal gas during a flight remains well below 0.001

198   When the mean free path increases at lower pressures there could be "wall-slip", non-zero

199   velocity at the wall which can be modeled as an effective decrease in viscosity increasing the

200   volume flow. Berg (2005) gives an approximate expression for the factor by which the flow

201   increases, $1 + 4 \, K_{slip} \, Kn$, where K_{slip} is a number close to 1 which depends on intermolecular

202   forces, and Kn is the Knudsen number, λ/d, with d being the internal diameter of the tube. At

203   high altitude, say 10 hPa, $\lambda \sim 7 \cdot 10^{-4}$ cm, so that Kn ~ 0.001 for d = 0.6 cm. For d = 0.3 cm the

204   flow would be increased by a factor 1.009 at 10 hPa.

205   When Kn becomes larger than ~0.01 a transition region of pressure is entered in which the flow

206   changes gradually from bulk flow of gases, laminar in our case, to molecular flow (O'Hanlon,

207   1980). In the latter flow regime the gas sample enters the tube as individual molecules, and gases

208   with higher molecular speed (lower mass) enter the tube more rapidly, so that the air sample may

209   not represent the composition of outside air, whereas in bulk flow an overwhelming fraction of

210   all molecules are equally swept along. As an example, for an AirCore with opening diameter of

211   0.3 cm this flow transition starts at a pressure altitude of ~2 hPa. Therefore, approximately 43

212   km might be the highest altitude that can be sampled with this diameter opening without first

213   quantitatively investigating molecular flow effects, although this limit depends also on the

214   sampling accuracy we require.

215 The above expressions for viscosity, $\eta \cong (1/3) \rho \, \mathbf{c} \, \lambda$, and heat conductivity, $\kappa \cong (1/3) \, c_v \, \rho_n \, \mathbf{c} \, \lambda$,
216 and similar for diffusivity, $D \cong (1/3) \, \mathbf{c} \, \lambda$ are approximate. More precise forms of these equations
217 vary depending on the treatment of intermolecular forces. Instead, we use a curve fit to empirical
218 data for viscosity in dry air as a function of temperature, as presented by Kadoya (1985). The
219 empirical data show, as expected, that there is no dependence on pressure in our range of
220 interest.

221 For diffusivity of trace gases in air as a function of temperature and pressure we use the
222 empirical equation presented by Massman (1999), $D(T,P) = D_0 \, (P_0/P) \, (T/T_0)^{1.81}$. D_0 is the
223 diffusivity, different for each trace gas in air, at 1 atmosphere air pressure (P_0) and 0 degrees
224 centigrade (T_0). This will be used when we calculate mixing of air samples entering the AirCore
225 sequentially. Mixing is caused both by molecular diffusion ($X_{rms} = (2Dt)^{0.5}$, see above) and by
226 the quadratic velocity profile of laminar flow, with zero speed at the wall and maximum speed in
227 the center. The latter is called Taylor diffusion (Karion, 2010), and is given by a diffusivity
228 constant $D_T = \mathbf{v}_{avg}^2 \, r^2 \, /(48 \, D)$ which has the same dimensions as D, $m^2 \, s^{-1}$.

229

4. Calculated in- and outflow results for some flights

231 In Figures 1− 4 the flight is shown of a small diameter (1/8 inch, internal diameter 2.92 mm)
232 AirCore (GMD008), with 93 m length and internal volume 619 cc, near Trainou, France (48.0
233 ^{o}N, 2.1 ^{o}E) on 20 June 2019. The ascent velocity of the helium balloon is nearly constant, while
234 the rate of mass outflow decreases steadily as a function of time as the pressure outside and
235 inside the AirCore drops. The descent velocity with parachute accelerates nearly linearly in the

236
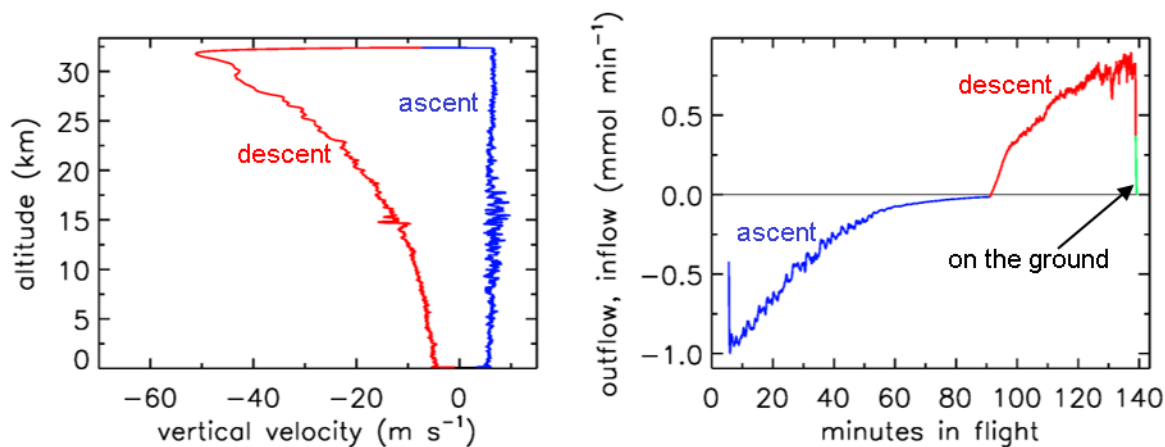
Figure 1. Descent velocity (negative) and rate of fill air outflow followed by air sample inflow
during flight of GMD008.

239 first 10 seconds to about 50 m s^{-1} as the air density at high altitudes is too low for air friction to
240 slow it down enough. The initial descent can be a chaotic tumble until the parachute gets a

241 "grip". Outflow and inflow are calculated with the fill dynamics program described below in
242 section 8.
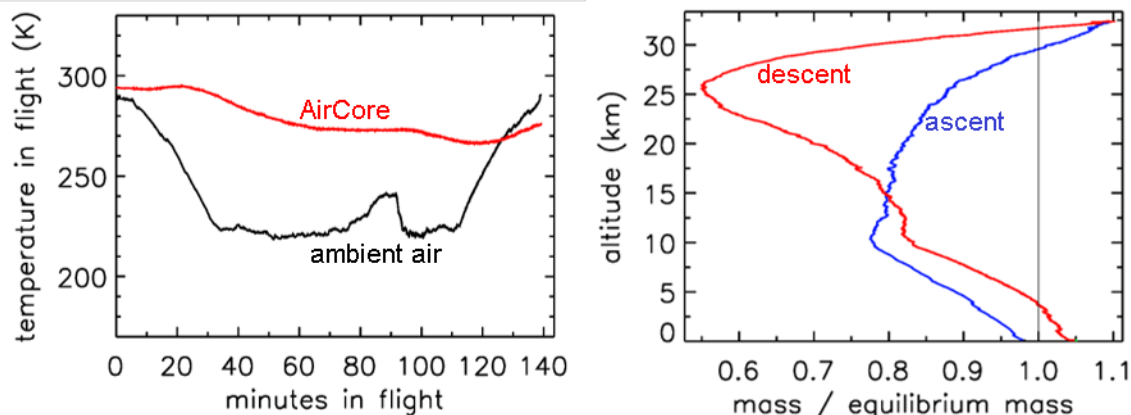
244 *Figure 2. Flight of GMD008. Left panel: Temperatures in degrees Kelvin. Right panel: How far*
245 *the mass inside the tube is out of equilibrium with ambient air.*

246 In Fig. 2 the outside air temperature first cools while in the troposphere, then becomes nearly
247 constant in the tropopause, and starts increasing again higher into the stratosphere. GMD008 was
248 well insulated but still partially followed the outside temperatures with a delay. In the right panel
249 the total amount of air in the tube is plotted relative to how much it would be if it had the same
250 pressure and temperature everywhere in the tube as the outside air. Vertical line: the ratio equals
251 1 if they were the same. During ascent in the troposphere (up to about 10 km) the air in the tube
252 is warmer, and thus less dense, than outside air. In the tropopause the tube continues to cool so
253 that the "deficit" becomes smaller, but at higher altitudes, around ~25 km the amount by which
254 the pressure in the tube is higher than outside becomes substantial relative to the low outside
255 pressure – as a result the ratio at ~34 km altitude becomes a bit larger than 1. Then, during
256 descent the outside pressure increases rapidly and the inflow cannot keep up because the
257 viscosity of air at low pressure is the same as at 1 bar (see section 3). Back in the troposphere the
258 tube warms up, but much more slowly than outside air. When the tube hits the ground, it is
259 colder than ambient air temperature so that the ratio is greater than 1.

260 In Fig. 3 the fill rate is plotted (mol per hPa of ambient pressure gain) divided by the final fill
261 (moles of air) at valve closure. At sea level the final pressure is close to 1013 hPa, so that the
262 average fraction of final fill amount per hPa will be approximately 0.001. The uptick upon

263

264
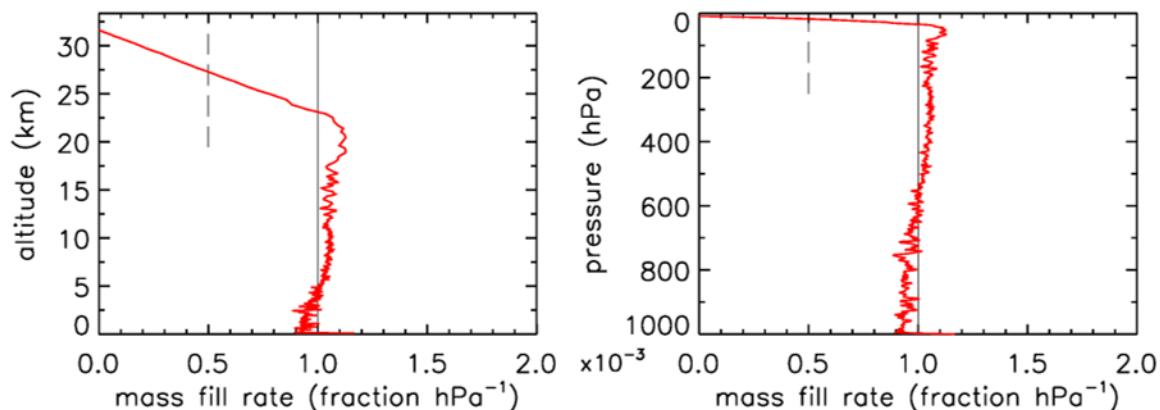
Figure 3. Flight of GMD008. The vertical line at 1.0 10⁻³ is approximately the expected rate of
sample inflow. The dashed line at 0.5 10⁻³ represents the half-fillrate point (see main text).

landing (very close to the x-axis) is the result of a bit of air still entering the tube initially while
ambient pressure stops changing, neglecting high frequency noise. If the valve is not closed
quickly this will reverse because as the tube warms up on the ground, the last air that came in
will be expelled. At high altitudes it takes time for the fill to start because ambient pressure
needs to build up enough to force the air in. The highest altitude was 32.4 km, at 7.7 hPa ambient
pressure. The fill starts at 31.6 km and pressure 8.5 hPa, slowly at first, and gradually becomes
faster. To compare the start of fill between AirCore designs with different diameters and valves,
we could take the point at which the fill rate is 0.5 10⁻³. In this case the "half-fillrate point" is at
27.3 km and ambient pressure of 17.3 hPa. We will see below that the fill starts much faster with

276
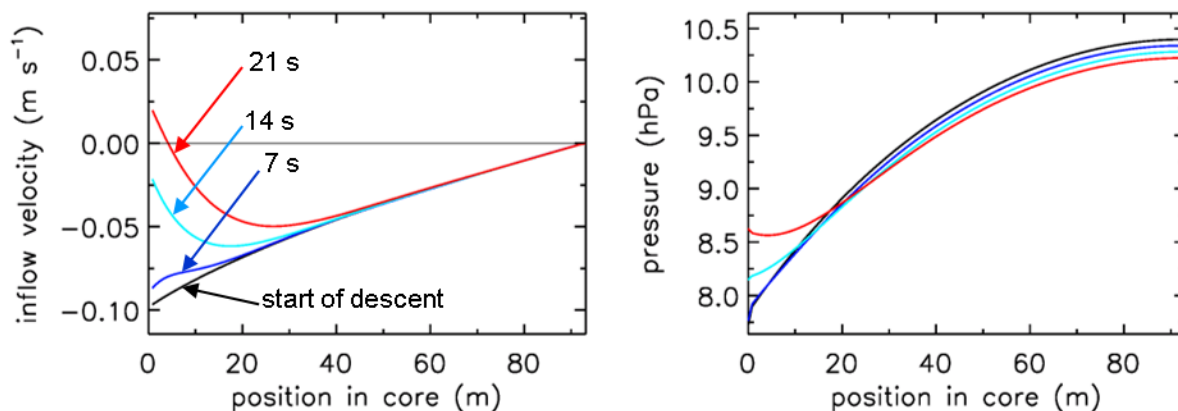
Figure 4. Flight of GMD008. The turnaround at high altitude. Inflow velocity and pressure
inside the AirCore from the moment the ascent stops and descent begins. Times are in seconds
after start descent.

larger diameters. Fig. 4 shows detail of flow and pressure inside the tube for the flight on 20 June
2019 at the start of descent. Initially the inflow velocity is negative. It is outflow, zero at the
closed end and increasing toward the open end. After 14 seconds into the descent (light blue

283 curve) the outflow has weakened considerably and the pressure gradient near the open end is
284 much smaller. Inflow starts after 19 s, very slowly at first, while at the same time the flow in
285 most of the tube is still negative (outflow toward the open end), consistent with the pressure
286 gradients.

287 Let us look now at an AirCore with larger diameters (Fig. 5). This one had 26 m of 1/4 inch
288 (internal diameter 5.84 mm) tubing at the open end and 37.6 m of 1/8 inch (2.67 mm internal
289 diameter) tubing at the closed end, with a total internal volume of 890 cc. The high-altitude fill
290 history of the two AirCores is summarized in Table1. In front of the open end was a valve, the
291 dryer (large magnesium perchlorate particles), and then another valve connecting to the AirCore
292 tube. It was flown in Oklahoma, U.S. (37.2 N, 97.8 W), on 23 July 2013. While the
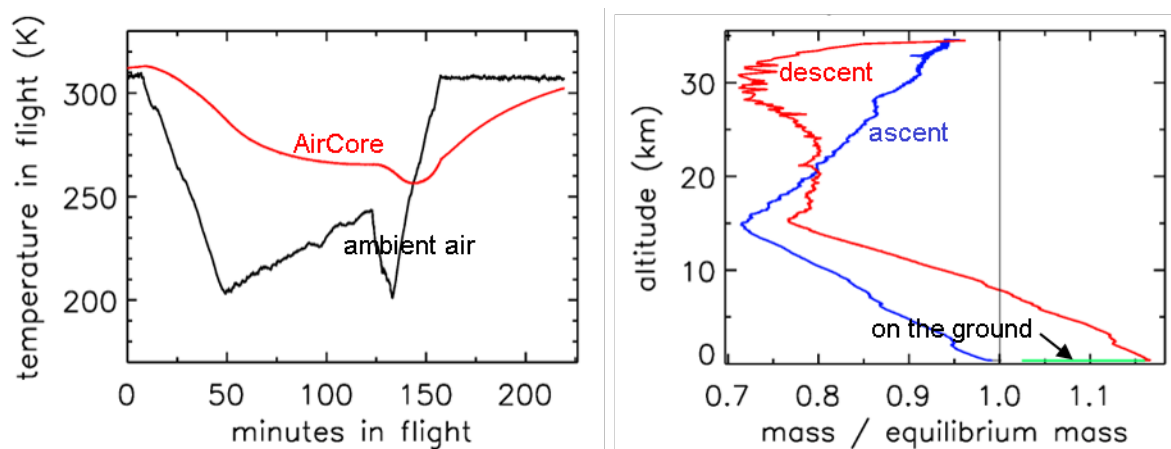
293

294 *Figure 5. Flight of AC01 in Oklahoma.*

295 AirCore used near Trainou, France, experienced a temperature range 15 K, the less well
296 insulated AC01 in Oklahoma saw a range of 57 K. At the moment of landing the average
297 temperature of the tube was ~40 K cooler than ambient. Fig. 5 shows the flight data until the
298 moment of valve closure. The valve remained open for 62 minutes after landing, so that the
299 lowest portion of the atmospheric sample, between pressure altitudes of 844 and 967 hPa (1565
300 to 352 m), was expelled as the AirCore warmed up. The descent started at 34.6 km altitude
301 (4.6hPa). The lowest relative mass deficit (~27%) was reached around 30 km, in contrast to the

302   Trainou flight with 50% at 27 km altitude respectively. The half-fillrate point of
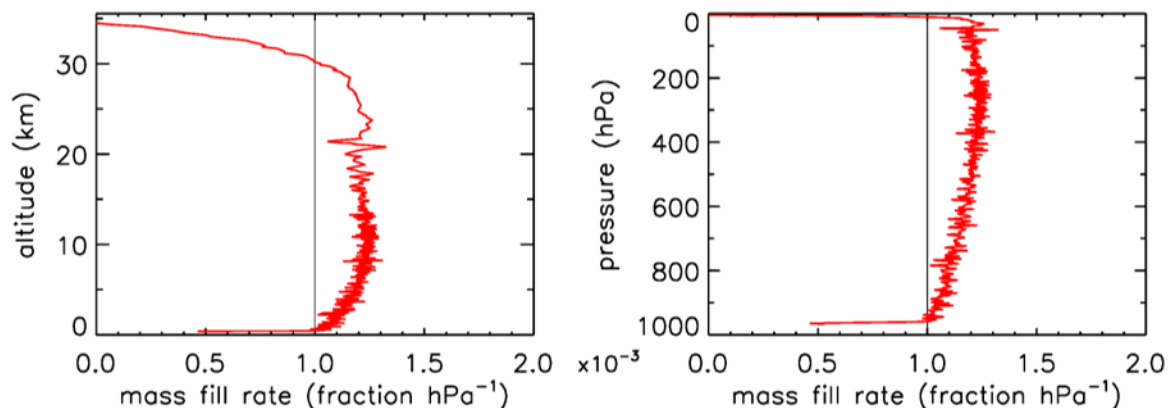
303

304   *Figure 6. Flight of AC01 in Oklahoma. Compare with Figure 3.*

305    $0.5 \ 10^{-3}$ per hPa is reached at 33.2 km altitude and 6.2 hPaof ambient pressure, a sampling
306   altitude gain of almost 6 km compared to the Trainou flight. If the total amount of initial fill air
307   that remained in the tube can be carefully measured it would give an independent estimate of the
308   pressure altitude where the fill (slowly) started. . The fill rate below ~8 km falls off noticeably
309   as the warming rate of the tube speeds up. The negative mass fill rate while on the ground cannot
310   be portrayed in Fig. 6 because ambient pressure remains constant. This AirCore design contains
311   a larger fraction of stratospheric air than GML008, mostly because of the wider diameter, but
312   also because it was allowed to cool more.
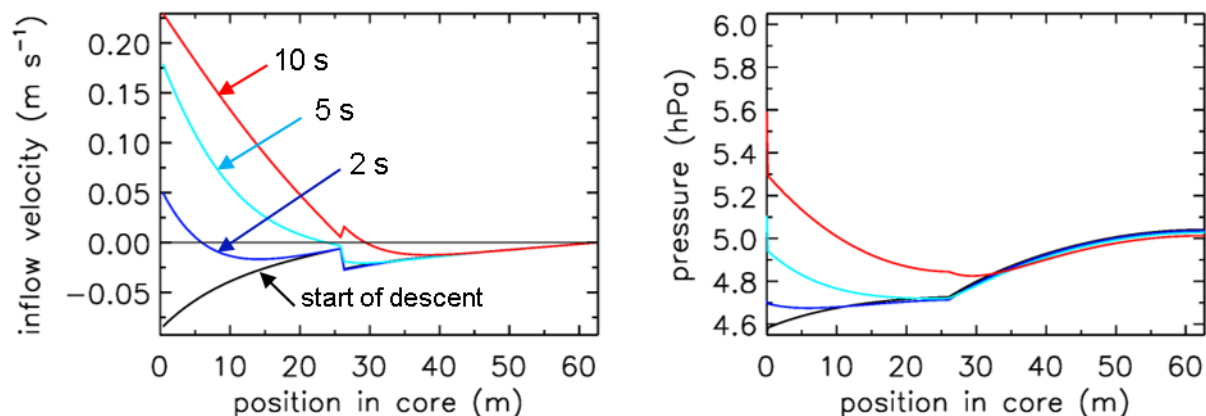
313

314   *Figure 7. Flight of AC01 in Oklahoma, showing inflow velocity and pressure gradients.*
315   *Compare with Fig. 4. Note the much smaller fill delay than in Fig. 4. The pressure drop across*
316   *the two valves and dryer is visible here.*   If one wants to sample still higher into the stratosphere
317   the diameter of the first 10 to 20 m at the open end needs to be widened further than 6 mm
318   diameter (Table 1). All of this is consistent with

319   Table 1. Comparison of start of fill process for two AirCore configurations

AirCore Trainou 2019	Int. Dia (mm)	Length (m)		Aircore Oklahoma 2013	Int. Dia (mm)	Length (m)
Aircore tubing	2.16	0.76		AirCore tubing	5.84	25.9
AirCore tubing	2.92	91.5		AirCore tubing	2.67	36.6
AirCore tubing	2.16	0.76				
internal volume		619 cc		internal volume		890 cc
Fill history	Time (s)	Altitude (hPa),(km)		Fill history	Time (s)	Altitude (hPa), (km)
start descent	0	7.7, 32.4		start descent	0	4.6, 34.6
start fill	19	8.5, 31.6		start fill	2	4.7, 34.4
half fillrate	123	17.4, 27.3		half fillrate	7	6.3, 33.2
full fillrate	266	34.2, 23.1		full fillrate	58	10.4, 30.2

320

Fig. (7), where we also see that at the start of the descent the outflow velocity inside the tube drops by a factor of ~ 4 when, moving from the back to the open end, at 25.9 m the tube diameter becomes wider by a factor of ~ 2. This applies of course also to the inflow as shown by the red curve. At the same point the pressure gradient becomes less steep by the same factor of 4. The fill starts at ambient pressure of 4.7hPa. We also note that in this case the pressure drop inside the two valves and the dryer is a large part of the overall pressure drop across the entire tube, an effect that becomes more pronounced as the tube diameter gets larger.

In these calculations I have experimented with another strategy to fill the AirCore. One could launch it with both valves open, but the one in the back is closed as soon as the descent starts. That would decrease the amount of fill air that remains in the back. However, the difference from having the back valve closed during the entire flight is negligible.

5. Valves

So far the treatment of valves and the dryer has been missing from this description. As a first approximation we could treat the valves as short pieces of tubing with reasonably "average" internal diameter and length such that their internal volume is correct. This does not provide enough flow resistance, when we compare it to differential pressure measurements made during flights between the closed end of the AirCore and the outside ambient air (Fig. 8).

339
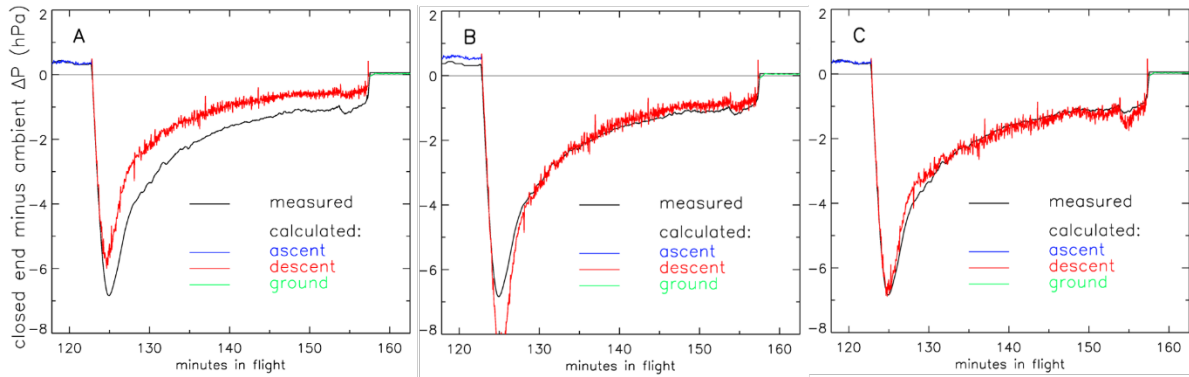
Figure 8. Pressure difference (ΔP) *between closed end of tube and outside air during the descent portion of flight of AC01 in Oklahoma as a function of elapsed time in flight. Black: measured pressure difference (hPa). Red: calculated* ΔP *with three different treatments of the valves.* A, *fixed internal diameter and length;* B, *same as in* A, *but optimized;* C, *using optimized* Cv *and X$_{TPR}$ (see main text) values.*

In panel A we calculate that during the descent the air enters the tube too easily, so that the altitudes assigned to the air sample in the stratosphere would be biased high. We could decrease the chosen internal average diameter (not a well-defined value) of the valves (panel B), optimized so that the difference between calculated and measured ΔP during the entire descent, from minute 123 to 157, is minimized. However, it is clear that this effective or apparent internal diameter needs to change during the flight. Using Cv values and a description of choked flow is clearly better. In panel C we have chosen the Cv and X$_{TPR}$ (see below) values such that the average difference from minute 123 to 157 is zero and the standard deviation of differences is minimized. This implicitly includes any effects caused by the dryer in between the two valves.

The flow inside a valve can be complicated, with sharp corners, turbulence, sudden acceleration through a flow restriction with its associated heating and cooling of the gas, etc. The industry has introduced flow coefficients (Cv in the U.S., and Kv elsewhere) as an empirical approach to flow calculations, as in the Swagelok brochure (2020). The expressions for air, slightly generalized from Swagelok, for gas flow are as follows. For low pressure drop flow, we have

$$Q_n = 6950 \ C \ v \ P_1 \left(1 - \frac{X}{3\,X_{TPR}}\right) \sqrt{\frac{X}{T_1}}$$

(Eq. 5a), where Q$_n$ is in liters per minute at standard conditions of 1 bar and 0°C, P$_1$ and T$_1$ are pressure (bar) and temperature (Kelvin) upstream of the valve, ΔP is the pressure drop across the valve, X is the pressure drop ratio ΔP/P$_1$, and X$_{TPR}$ is the terminal pressure drop ratio between (0 and 1) above which we have choked flow. Under choked flow conditions the flow is fully independent of P and T downstream of the valve. It is also important to know that the flow coefficient Cv is not a pure number, but has physical quantities and units embedded in it.

367   For a high pressure drop $(X > X_{TPR})$, we have

368    $Q_n = 6950\ C\ v\ P_1\ \frac{2}{3}\ \sqrt{\frac{X_{TPR}}{T_1}}$ (Eq. 5b), which is obtained from the previous expression by
369   substituting X_{TPR} (a constant) for X. In these expressions we prefer to express the flow, instead
370   of in standard L/min as in the Swagelok brochure, as 0.04403 mol/min. This is the same, when
371   using the molecular weight of dry air (28.97 g/mol), as a mass flow of 1.276 g/min.

372   In Fig. 8C we optimized both Cvand X_{TPR} to get the best match for the calculated pressure
373   difference across the AirCore with the observed history during the descent. The value of X_{TPR}
374   depends on valve design, and may not be the same when flow goes in the opposite direction.
375   Many valves have an arrow for flow direction printed on them. For many AirCore flights
376   differential pressure measurements have not been recorded. However, the valves (and also
377   dryers) could be tested with a standard procedure (see Fig. 9 as one example). Alternatively, or
378   as a complementary check, a micro-spiking method during filling could be used (Wagenhäuser,
379   2021).

380   Figure 9 shows a potential test procedure for determining Cvand X_{TPR} values. The figure is
381   drawn using the two expressions for Q_n above, for low flow and choked flow. Starting from a
382   uniform pressure of 1 bar, the pressure at the downstream side is lowered in 10 hPasteps, at 2 s
383   intervals. In this example $Cv = 0.01$ and $X_{TPR} = 0.5$, so that the transition to choked flow occurs
384   at a pressure drop of 0.5 bar (panel A, upward arrow at 100 s). When the pressure at 10 m
385   approaches zero, the flow speed is high, causing a significant pressure drop between 5 and 10 m.
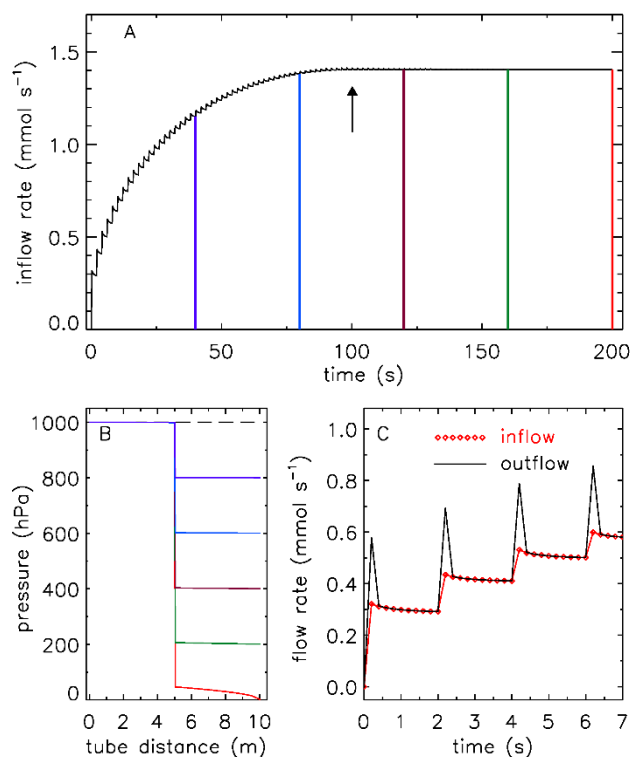
386

387 *Figure 9. A potential test procedure to determine Cv and X_{TPR} values for valves. In this example*
388 *there is 5 m of ¼" tubing (ID 5.84 mm) on each side. Outflow at the 10 m point (black curve) is*
389 *shown in panels A and C. There is a flow pulse at every step because the downstream 5 m*
390 *section empties quickly. The time resolution is 0.2 s. Inflow at 0 m is shown as red diamond*
391 *symbols in panel C. Panel B, pressure in the tube from time 0 (dashed line) at 40 s intervals,*
392 *corresponding to the colors in panel A.*

393

6. Mixing inside the tube

395 The fill dynamics calculation has produced time series of air density, pressure and temperature,
396 and flow velocity everywhere in the tube as a function of time, from the start of the fill process,
397 which begins a varying amount of time after the AirCore has started its descent, to the time of
398 valve closure. We divide the final amount of air in the tube at closure into 400-500 equal mass
399 packets. Starting from 400 we increase the number, which shrinks the size of each packet, until
400 the remaining fill air in the back of the tube comprises an exact integer number of packets. For
401 each mass packet, after it has entered the tube we follow it through the tube, as it is pushed
402 toward the back while being compressed by packets entering later. The time steps are defined by
403 when a new packet has fully entered, and they are longer at the start of the fill. The molecular
404 diffusivity D and the Taylor diffusivity D_T are different at each step. However, the amount of
405 spreading of a packet calculated at each time step "k" is decreased as the increasing pressure
406 compresses the packet further. So the contribution of each step to the final spreading at valve
407 closure is calculated by dividing the density during that time step by the final density in the tube.
408 We are thus accumulating the "2Dt" term of $X_{rms} = (2Dt)^{0.5}$, with Taylor diffusion added:

409
$$X_{rms} = \sqrt{2 \; \sum_k (D_k + D_{T,k}) \frac{\rho_k}{\rho_{final}} \; t_k} \qquad\qquad Eq. 6$$

410 For an AirCore with (almost) uniform diameter we get mixing as in Fig. 10 A. Close to the open
411 end at position 0 m, there is very little mixing because the time to mix was short. Near the closed
412 end at 93 m the spread of mixing deviates from what see in the first approximately 2/3 of the
413 tube because the fill started slowly, giving extra mixing time for the high altitude samples that
414 were later pushed to the back.
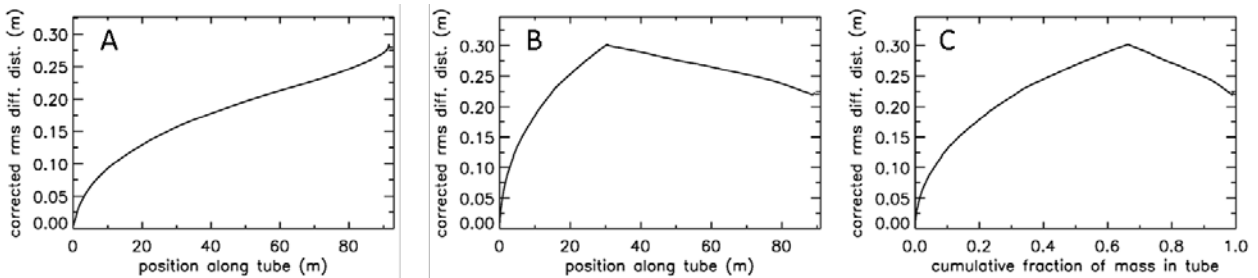
415

416 *Figure 10. Root-mean-square diffusive mixing when the valve at position 0 is closed. Panel A,*
417 *Flight of GMD008 in Trainou. Panel B, the same flight data, but used to calculate the filling of a*
418 *different AirCore, with 30.9 m of 1/4" tubing at the open end, and 60.1 m of 1/8" at the closed*
419 *end. Panel C, same as B, but plotted as cumulative fraction of total mass, from 0 to1.*

420 For an AirCore with two sections of different diameter we see an interesting effect (Fig.10 B).
421 The air that comes in at high altitudes and ends up in the back of the tube, has to go through
422 the1/4" section first. When a packet enters the 1/8" section, its spread becomes approximately
423 four times larger, while its 2Dt accumulation term stays the same. Approximately, because the
424 inner diameters (ID) matters, not the outer (OD). To correct for the jump we add another factor
425 to Eq. 6, and we will call this corrected rms diffusion distance:

426
$$X_{rms} = \sqrt{2 \; \Sigma_k(D_k + D_{T,k}) \frac{\rho_k}{\rho_{final}} \frac{(dvol/dx)_k}{(dvol/dx)_{ref}} \; t_k}$$
Eq. 7

427 In Eq. 7 dvol/dx is the increment in volume per increment in length of the tube, while $(dvol/dx)_{ref}$
428 is the total volume divided by the total length, both in units of m^2. This prevents a jump at the 30
429 m position, but more importantly, what matters for mixing is the spread relative to total mass in
430 the tube, not whether it is in the 1/4 or 1/8" section. From now on we call this configuration "1/4
431 -1/8". Fig. 10 B shows that air closer to the back has been in the 1/4" section for a shorter time,
432 and thus experienced less mixing relative to mass. When plotting mixing not as a function of
433 position, but as a function of cumulative mass in the tube, Fig. 10 C also shows that the 1/8"
434 section contains approximately 1/3 of the total air sample.
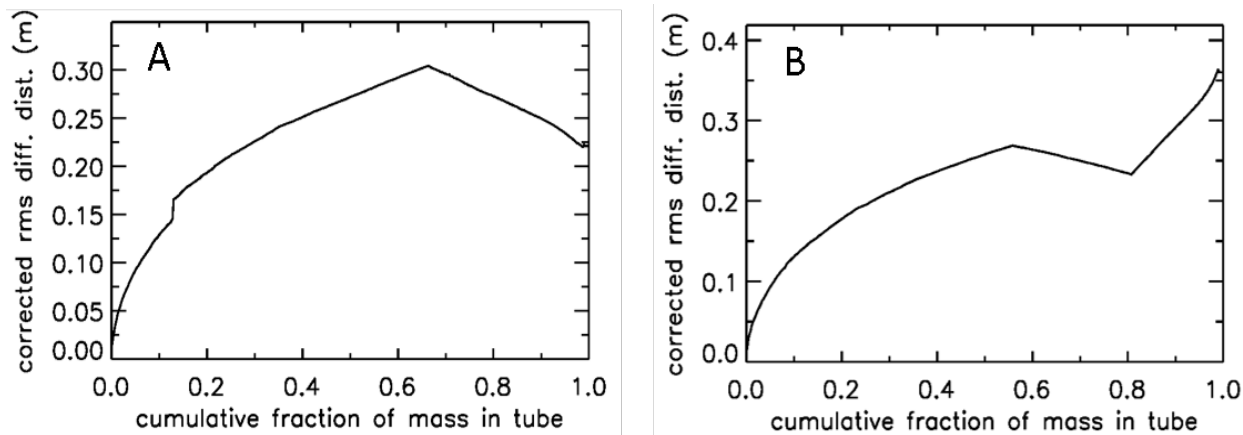
435
436 *Figure 11. Two additional cases of mixing upon valve closure. Panel A, same AirCore 1/4 -1/8,*
437 *but the flight data have been changed. Panel B, same flight data as in Fig. 10A, but the AirCore*
438 *configuration is 1/4 - 1/8 - 1/4.*

439 In Fig. 11A when the tube had descended to 850 mb, the atmospheric pressure data were
440 changed to simulate an updraft (lowering outside pressure) followed by a downdraft. The most
441 recent 7 mass packets were lost from the tube during the updraft, and replaced by new air during
442 the downdraft (above average rate of increase of outside pressure). As a result, the air sample

443   that just escaped from being lost is now adjacent to the replacement air, creating the jump in rms
444   mixing because it has been ~15 s longer in the tube than the first replacement air entering. In Fig.
445   11B the AirCore has now three sections, from the open to the closed end, first 30.1 m of 1/4",
446   then 52.1 m of 1/8", and 10.1 m of 1/4" diameter, which we will call "1/4 - 1/8 – 1/4". This was
447   done solely to illustrate clearly the effects of using different diameters. Similar to what we saw in
448   Fig. 10A, the spread of mixing steepens near the closed end. Also those samples resided not long
449   enough in the 1/8" section to have much benefit in terms of slowing down the mixing, but
450   between 0.80 and 0.85 they had been long enough in the 1/8" section to have experienced less
451   mixing than air ending up at the 0.57 point, the first transition between 1/4 and 1/8".

452   We will now express the amount of spreading (in both directions – twice the rms distance) of
453   each equal-mass "packet" of air as a fraction of the total mass of air in the tube, assuming that
454   the temperature inside the tube has become uniform. If that fraction were 0.01 everywhere in the
455   tube there would be slightly less than 100 independent samples in the AirCore. Slightly less
456   because the remaining fill air in the back takes up space. Fig. 12 shows a more realistic situation.
457   Each sample takes up the same volume, separated by the blue vertical lines, producing vertical
458   boxes. If there is almost no mixing, as in the case of the last sample that entered the AirCore, the
459   sample almost completely fills the first volume (or box in Fig. 12A), which is indicated by the
460   value 1.0 on the y-axis. The red curve centered on the second box has started to "leak" some
461   sample into the adjoining boxes. The next samples shown are the 7th, 12th, and 17th. For the latter,
462   the sample is just starting to leak into boxes 15 and 19. To plot the start of this process correctly,
463   each packet is subdivided into 13 equal portions. Narrow Gaussian spreading, slowly increasing
464   further into the tube, is calculated for each portion, and then summed. The width of each
465   Gaussian is shown in Fig. 10C as a function of fraction of cumulative mass in the tube, and the
466   area of each curve is 1/13 of the area of the box. This produces a constant value of 1.0 in the
467   center and only the outer portions reach into the neighboring boxes.
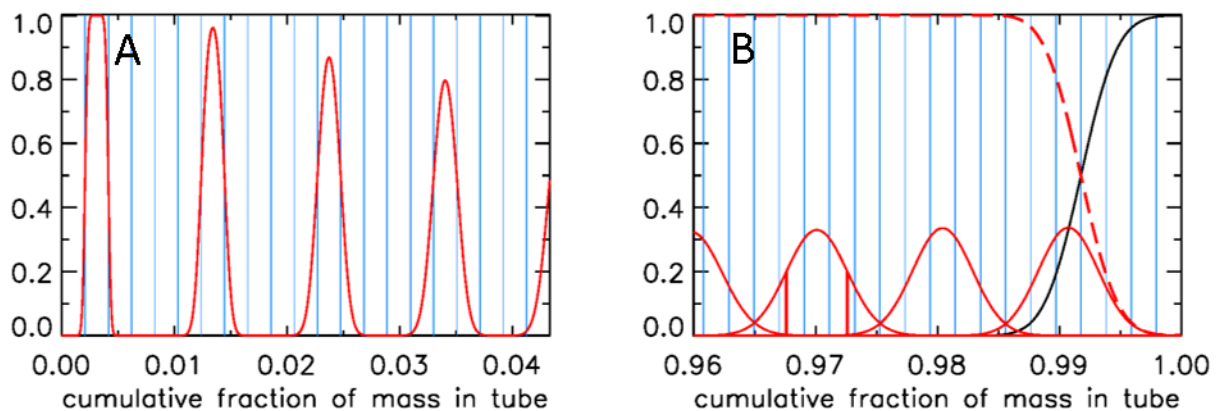
468

469   *Figure 12. A, Mixing of individual air "packets" (red) near the open end with their neighbors*
470   *after valve closure for the case shown in Fig. 10C; B, mixing near the closed end (red), vertical*

471 *red lines centered on 0.97 show the ± 1 σ points, black curve is remaining fill air, and the sum of*
472 *all actual sample packets, also of those not shown, is the red dashed line.*

473 In Fig. 12B we plot the situation near the closed end. As in Fig. 12A, the mixing of only every
474 fifth air packet is plotted, here ending with the first that came in at the highest altitude, centered
475 approximately at 0.991. The remaining fill air in this case has the mass of four packets, and the
476 curves of fill air and of the total air sample (sum of all packets) cross over at exactly the point
477 where the fourth box from the right starts. How we calculate mixing at a closed end (at x = 0) is
478 shown in Fig. 13.
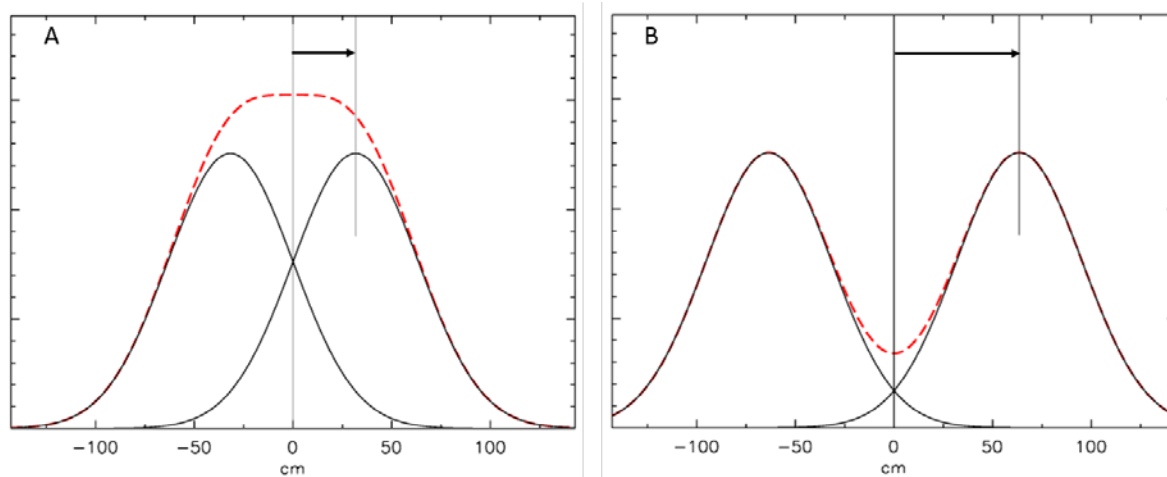
479

480 *Figure 13. Mixing at a closed end. The Aircore is to the right of the zero centimeter point. A, the*
481 *distribution of mixing started one hour ago from a plane at 31.8 cm (one root-mean-square of*
482 *the distribution), indicated by the arrow. A fictitious "mirror" distribution is centered at -31.8*
483 *cm. The red dashed curve is the sum of the two distributions; B, same calculation, but the center*
484 *of the distribution is twice as far from the end as in A.*

485 Diffusive mixing that would be to the left of x = 0, is reflected toward positive values of x. The
486 slope of the distribution must be zero at x = 0 because any non-zero slope would imply a
487 diffusive flux out of, or into, the tube. This is conveniently modeled by assuming a fictitious
488 distribution mirrored relative to x = 0, then the two are added, and the portion of the sum for
489 positive values of x represents the mixing distribution near a closed end.

490 Let us assume that after the valve has been closed there has been a half hour delay before
491 analysis starts. Therefore, additional diffusion has taken place, as shown in Fig. 14 for the case
492 1/4 - 1/8 –1/4 (Fig. 11B). The 2Dt term has been increased by an amount dependent on the
493 diameter of the tube, normalized as in Eq. 7. In the upper right (panel B) the square root of the
494 sum has been taken, and then transformed into the spreading width relative to total mass in the

495
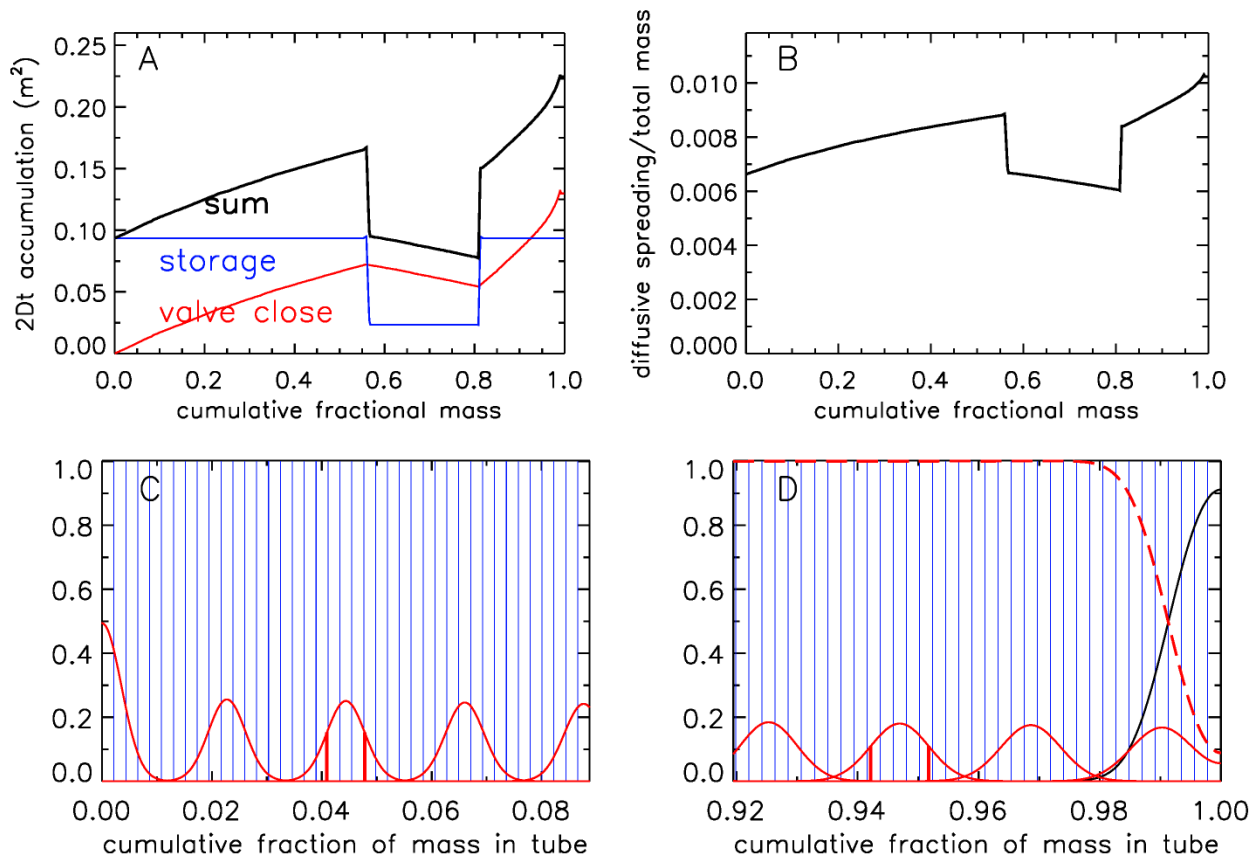
Figure 14. Mixing after 30 minutes of storage, for AirCore 1/4 - 1/8 -1/4. A, Sum (black) of the 2Dt accumulation during the flight (red) and during storage (blue), in units of m^2; B, spreading width expressed as a fraction of total mass in the tube; C, amount of spreading near what was the open end, for clarity only every 10th packet is shown; D, same, near the closed end. Vertical red lines show the $\pm 1\,\sigma$ distances from the peak.

tube. The width is defined here as the distance between the $\pm 1\,\sigma$ points of the Gaussian which contains ~68% of the probability distribution, shown in Fig. 14C at x = 0.0410 and 0.0478 around the center at x = 0.0444, and in fig. 14D at x = 0.9422 and 0.9518 around the center at x = 0.9470. These numbers correspond to the full widths shown in fig. 14B. The last packet to enter the tube is centered at x = 0.0011 and $1\,\sigma = 0.0033$. Most of the diffusive spreading is to the right, so that the peak is almost twice as high and the full width a little over half as wide as the one centered on x = 0.023.

Often the AirCore is analyzed significantly later than 30 min. after valve closure, and the measurement process itself may take half an hour. In Fig. 15 the state of mixing four hours after valve closure has been calculated, and two AirCore configurations are compared. The

512
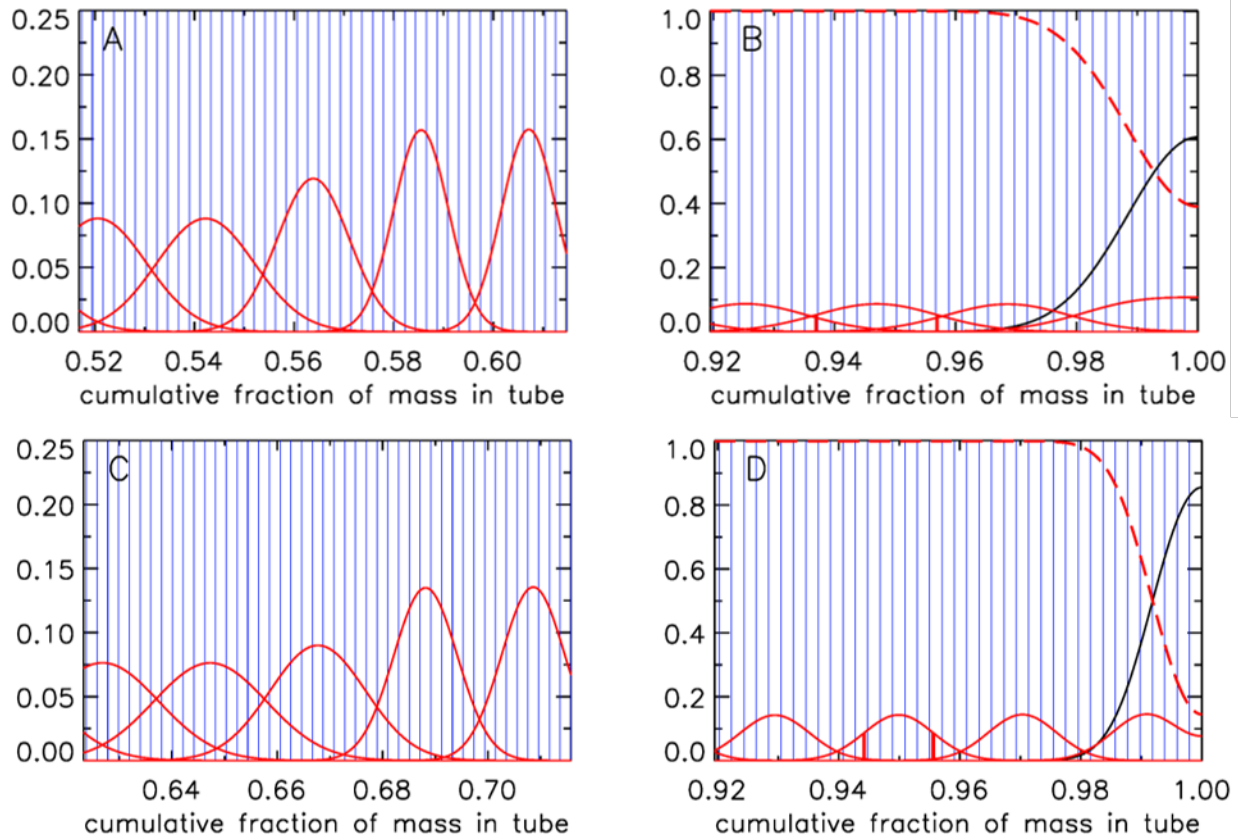
Figure 15. Mixing after 4 hours of storage. A, at the transition from1/4" diameter to 1/8", for AirCore 1/4 - 1/8 - 1/4; B, near closed end, for 1/4 - 1/8 - 1/4; C, at the transition from 1/4" diam. to 1/8", for AirCore 1/4 - 1/8; D, near closed end, for 1/4 - 1/8.

spreading width of air "packets" near the closed end is nearly twice as large for the 1/4 - 1/8 – 1/4 case as for the 1/4 - 1/8 case, and the initial fill air penetrates almost 50% further into the tube. It would in most cases not be a good idea to have a wide bore section at the closed end. If one waits 24 hours (6 times longer) before starting the analysis, the spreading width near the closed end, centered at x = 0.9470, is 2.32 times larger than after 4 hours, not quite √6 because after 4 hours the spreading that occurred during the descent still makes a small, but still noticeable, contribution.

7. Potential information content of the AirCore

The mixing calculated above allows for a realistic and precise estimate of the altitude resolution of the full air sample, both when the AirCore is analyzed in the field promptly after landing, or hours or even days later. When the air is slowly pushed through an analyzer, we obtain a quasi-continuous curve for the mole fraction of the gases of interest as a function of fractional cumulative mass in the tube which is linked to flight data such as pressure altitude, geometric

530   altitude, latitude, longitude, etc. as calculated from the filling dynamics. We define the
531   information content as the number of independent air samples that are inside the tube, or the
532   number of degrees of freedom (DoF). Longer wait times before analysis decrease DoF.For
533   example the small Trainou AirCore (619 cc, Table 1) has DoF of 154, while after waiting four
534   more hours before analysis DoF has dropped to 67. DoF could be decreased further by
535   additional mixing in the measurement cell, or by successive analyzer cells measuring different
536   gas species. In the section above we chose more than 400 equal mass packets to calculate
537   mixing. This was done to prevent a possibly low numerical resolution of the mixing calculation
538   which would unnecessarily create a low bias in DoF estimates. Ideally, the measurement process
539   could be modeled in a way similar to the fill and mixing calculation above, convolving the
540   packets leaving the AirCore with a pulse response of the measurement cell. The response could
541   be measured separately by introducing a sharp spike just before the cell, and recording how it is
542   mixed and flushed out. This would be similar to the spiking method described by Wagenhäuser
543   et al. (2021). In the worst case the measurement cell would be perfectly mixed giving rise to
544   exponential flushing. In that case, after one cell volume has entered from the AirCore into the
545   measurement cell, the latter still contains a fraction 1/e of what went through the cell before, so
546   that the new volume comprises $(1 - 1/e) = 0.63$ of the cell loading. On the other hand, "plug
547   flow" (like in the AirCore itself) would produce very little additional mixing, but there could still
548   be some turbulent eddies near the entrance and exit of the cell. The actual influence of the
549   measurement cell on mixing lies somewhere in between those two extremes.

550

8. Numerical implementation

552   The AirCore can consist of one or more sections of different length, each with a different inner
553   diameter. For example, GML has flown AirCores with a wider bore at the open end and a narrow
554   bore at the closed end, in order to get better vertical resolution for the stratosphere. The sections
555   can be divided into a number of smaller segments when Eq. 2 is discretized for numerical
556   solution (Fig. 16):

557
$$Q = -\rho \frac{\pi r^4}{8\eta} \frac{dP}{dz} \implies Q_j = -\frac{P_j + P_{j+1}}{R(T_j + T_{j+1})} \frac{\pi r_j^4}{8\eta_j} \frac{P_{j+1} - P_j}{dz_j}$$

558   Q_j is centered in the middle of segment dz_j. The first factor in Q_j is the average amount density
559   (ρ_j). The pressure change at the boundary between segments dz_{j-1} and dz_j caused by the
560   imbalance of the flows Q_{j-1} and Q_j is equal to that imbalance divided by the volume between the
561   mid points of dz_{j-1} and dz_j. Adding in the pressure change due to temperature (Eq. 2) we get for
562   the change at boundary j:

563
$$\frac{dP_j}{dt} = \frac{P_j}{T_j} \frac{dT_j}{dt} + \frac{T_j}{0.5(dz_{j-1}r_{j-1}^2 + dz_j r_j^2)} \frac{P_j + P_{j+1}}{T_j + T_{j+1}} \frac{r_j^4}{8\,\eta_j} \frac{P_{j+1} - P_j}{dz_j}$$

564
$$-\frac{T_j}{0.5\left(dz_{j-1}r_{j-1}{}^2 + dz_j r_j{}^2\right)} \frac{P_{j-1} + P_j}{T_{j-1} + T_j} \frac{r_{j-1}{}^4}{8\,\eta_{j-1}} \frac{P_j - P_{j-1}}{dz_{j-1}} \qquad \text{Eq. 8}$$

565
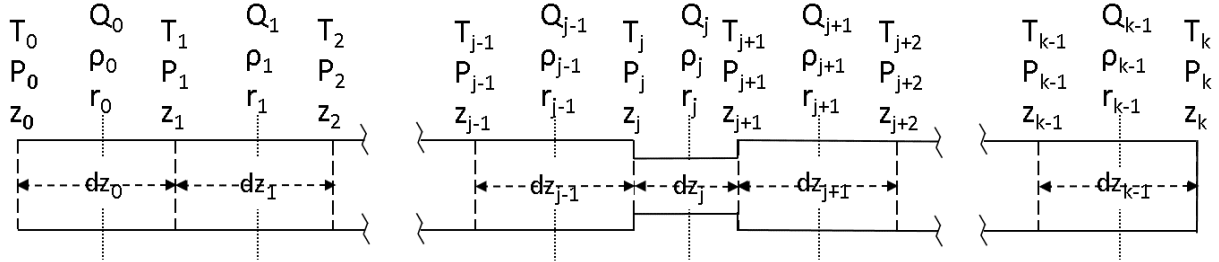
566

567 *Figure 16. Coordinate system in the AirCore. The coordinate along the length of the tube is z (m).*
568 *There are k segments, starting from the open end at z_0 to the closed end at z_k, between the*
569 *vertical dashed lines. Amount flow (Q_n, mol s^{-1}), amount density ρ_n (mol m-3), simply written as*
570 *Q and ρ from here on out, are defined in the middle of each segment, pressures (P) and*
571 *temperatures (T) are defined at the borders of each segment. The length (dz) as well as radius*
572 *(r) of the segments may differ.*

573 The first term (P/T)(dT/dt) is handled separately from the two other terms describing the amount
574 change. We write the latter two with the time step going from n to n+1 (superscript):

575
$$P_j^{n+1} - P_j^n = \left[\frac{2T_j^n\left(P_{j+1}^n + P_j^n\right)}{T_{j+1}^n + T_j^n} \frac{r_j^4}{\eta_j} \frac{P_{j+1}^{n+1} - P_j^{n+1}}{dz_j}\right.$$

576
$$\left. -\frac{2T_j^n\left(P_{j-1}^n + P_j^n\right)}{T_{j-1}^n + T_j^n} \frac{r_{j-1}^4}{\eta_{j-1}} \frac{P_j^{n+1} - P_{j-1}^{n+1}}{dz_{j-1}}\right] \frac{t^{n+1} - t^n}{8\left(dz_{j-1}r_{j-1}^2 + dz_j r_j^2\right)} \qquad \text{Eq. 9}$$

577 On the right hand side we have defined the pressure *differences* at the *end* of the time step. The
578 reason is to make the solution of the matrix equation described below unconditionally stable.
579 This method has been described as "fully implicit" or "backward time" (Press, 1992). We leave
580 the pressure and temperature *averages* as defined at the start of the time step. They determine the
581 average amount density of the air and do not create any numerical instability. Eq. 9 can be
582 further re-arranged, for j =1 to k-1, as

583
$$P_j^n = -\frac{t^{n+1} - t^n}{8\left(dz_{j-1}r_{j-1}^2 + dz_j r_j{}^2\right)} \left[\frac{2T_j^n\left(P_{j+1}^n + P_j^n\right)}{T_{j+1}^n + T_j^n} \frac{r_j^4}{\eta_j dz_j}\right] P_{j+1}^{n+1} +$$

584
$$\left(1 + \frac{t^{n+1} - t^n}{8\left(dz_{j-1}r_{j-1}^2 + dz_j r_j^2\right)}\right)\left[\frac{2T_j^n\left(P_{j+1}^n + P_j^n\right)}{T_{j+1}^n + T_j^n}\frac{r_j^4}{\eta_j dz_j} + \frac{2T_j^n\left(P_{j-1}^n + P_j^n\right)}{T_{j-1}^n + T_j^n}\frac{r_{j-1}^4}{\eta_{j-1}dz_{j-1}}\right]P_j^{n+1}$$

585
$$- \frac{t^{n+1} - t^n}{8\left(dz_{j-1}r_{j-1}^2 + dz_j r_j^2\right)}\left[\frac{2T_j^n\left(P_{j-1}^n + P_j^n\right)}{T_{j-1}^n + T_j^n}\frac{r_{j-1}^4}{\eta_{j-1}dz_{j-1}}\right]P_{j-1}^{n+1} \qquad \text{Eq. 10}$$

586   This is a tridiagonal matrix equation, $\mathbf{A} \cdot P^{n+1} = P^n$, linking the k+1 dimensional pressure vector
587   P^{n+1} at the end of the time step to the pressure vector P^n at the start of the time step. The solution
588   is $P^{n+1} = \mathbf{A}^{-1} \cdot P^n$, in which $\mathbf{A}^{-1}$ is the inverse matrix calculated by the subroutine TRISOL which is
589   the IDL version of TRIDAG described by Press et al (1992). If the tube is closed at z = 0, then in
590   the first line of $\mathbf{A}$ the first (diagonal) and second (above the diagonal) element (all others are
591   zero) are respectively

592
$$1 + \frac{t^{n+1} - t^n}{8\left(dz_0 r_0^2\right)}\frac{2T_1^n(P_1^n + P_0^n)}{T_1^n + T_0^n}\frac{r_0^4}{\eta_0 dz_0} \quad \text{and} \quad -\frac{t^{n+1} - t^n}{8\left(dz_0 r_0^2\right)}\frac{2T_1^n(P_1^n + P_0^n)}{T_1^n + T_0^n}\frac{r_0^4}{\eta_0 dz_0}$$

593   If the tube is open at z = 0, then the first element of the first line equals 1, and all others are zero.
594   In this case P_0 is defined at all times by the outside atmospheric pressure, or by a defined
595   pressure from a cylinder. There is no influence from any place inside the tube. The algorithm
596   also allows the other end to be either closed or open to outside air. If closed, then the last two
597   elements of the $(k+1)^{st}$ row are respectively

598
$$-\frac{t^{n+1} - t^n}{8\left(dz_{k-1}r_{k-1}^2\right)}\frac{2T_{k-1}^n(P_{k-1}^n + P_k^n)}{T_{k-1}^n + T_k^n}\frac{r_{k-1}^4}{\eta_{k-1}dz_{k-1}} \quad \text{and}$$

599
$$1 + \frac{t^{n+1} - t^n}{8\left(dz_{k-1}r_{k-1}^2\right)}\frac{2T_{k-1}^n(P_{k-1}^n + P_k^n)}{T_{k-1}^n + T_k^n}\frac{r_{k-1}^4}{\eta_{k-1}dz_{k-1}}$$

600   If both sides are open, each with a different defined constant pressure, then after an initial
601   transient the flow settles to steady state flow corresponding to Poiseuille's equation.

602   This describes the core algorithm, of which there are two versions, called tubeflowstep3.pro and
603   tubeflowstep3Cv.pro. They have been programmed in Interactive Data Language (IDL). These
604   algorithms have the flexibility to accommodate segments of the tube that have different lengths
605   as well as diameters, flows in both directions, one or two valves open, a temperature gradient
606   along the tube with its corresponding viscosity gradient, and variable time steps. Another
607   routine, called analyzefill_Gaus_ict.pro, reads the lengths and diameters of tube sections, valves
608   and dryer, and the relevant flight data, namely outside air pressure and temperature, the
609   temperature of the AirCore at different locations along the tube, all as a function of time. If Cv
610   and X_{TPR} values of valves are defined they will be used. In that case tubeflowstep3Cv.pro nudges
611   the apparent internal diameter of one or more valves for a given flow toward satisfying Eq. 5 (see
612   section 5). This needs to be iterated because when we change the internal valve diameter the
613   pressures and flows will then adjust elsewhere in the tube. The analyzefill_Gaus_ict program

614   also reads altitude, latitude, and longitude, but they are not needed for the flow dynamics
615   calculation per se. Analyzefill_Gaus_ict also sets up the coordinate system and initializes
616   variables. By calling tubeflowstep3.pro at every time step, or tubeflowstep3Cv.pro if Cv and
617   X_{TPR} values are defined, it calculates the pressure in the tube, the amount of air and the amount
618   flow, and the flow velocity, all as a function of time and location in the tube. This is how
619   altitude, pressure altitude, latitude, and longitude are tied to position in the tube. The _Gauss
620   portion of the name indicates that Gaussian mixing is used as described in this paper, and _ict
621   indicates that the program expects the needed information about the tube and the flight in the
622   ICARTT format.

623   Although developed simultaneously with analyzefill_Gaus_ict.pro for the passively filled
624   AirCore, the tubeflowstep3Cv program can also be used to model flow when the AirCore is
625   actively filled with a pump and some form of flow and pressure control. In that case a program
626   equivalent to analyzefill_Gaus_ict.pro would need to be developed.

627   The code in analyzefill_Gaus_ict.pro also produces diagnostic graphics showing how the fill
628   proceeded. In fact, all figures in this paper have been produced by analyzefill_Gaus_ict.pro
629   except for Figs. 9 and 13.

630

631   9. Some recommendations for improvements in the analysis of AirCores

632   Laboratory measurements of the flow properties of valves, as expressed in the flow coefficient
633   Cv and the terminal pressure drop ratio X_{TPR}, as well as the flow properties of dryers could be
634   helpful for further improving dynamics code as described in this paper, and will be especially
635   helpful for potential revisions of sample altitude assignments of older flights. For dryers,
636   permeability is a more important property than porosity.

637   The precision of the sample mixing estimates could be improved by laboratory measurements of
638   the pulse response of analyzers, especially when an AirCore is analyzed quickly in the field
639   because very little mixing has yet occurred for the air that came in last.

640   In addition to measuring the pressure inside the tube during a flight at the closed end, one could
641   consider measuring the pressure inside at a place closely behind the valve(s) plus dryer at the
642   open end. It does not need to be done routinely, but it would give a history of the total pressure
643   drop across the valve and dryer only.

644   In cases where people want to fly AirCores without a dryer it could be helpful to study wall
645   effects. Water vapor adheres tightly to many surfaces, and as anyone experienced with vacuums
646   knows, it is often hard to pry it off the walls. One possible experiment would be to inject a short
647   pulse of wet air at one end of a thoroughly dried tube and register what comes out at the other
648   end. How much stays behind, for how long? How does it affect other species? In general, wall

649 effects could make the AirCore into a (poor) gas chromatograph if gases have different
650 adsorption/desorption properties.

651

652 **Acknowledgement**

653 I thank Anna Karion, Colm Sweeney, Tim Newberger, Jack Higgs, Sonja Wolter, and Bianca
654 Baier of GML for making our lab's AirCore program blossom. Especially the controlled return
655 on a glider is a very promising improvement over the return by parachute.

656

657 The main fight analysis program and subroutines in the IDL language are available at
658 https://gml.noaa.gov/aftp/user/tans/AirCoreIDL/

659

660 **References**

661 Battle, M., M. Bender, T. Sowers, P. Tans, J. Butler, J. Elkins, J. Ellis, T. Conway, N. Zhang, P.
662 Lang, and A. Clarke (1996), Atmospheric gas concentrations over the past century measured in
663 air from firn at the South Pole, Nature 383, 231-235.

664 Berg, R. (2005), Simple flow meter and viscometer of high accuracy for gases, Metrologia 42,
665 11-23.

666 Chapman, S. and T. Cowling (1970), The mathematical theory of non-uniform gases, 3rd edition,
667 Cambridge University Press.

668 Jeans, J. (1952), An introduction to the kinetic theory of gases, Cambridge Univ. Press.

669 Kadoya, K., N. Matsunaga, and A. Nagashima (1985), Viscosity and Thermal Conductivity of
670 Dry Air in the Gaseous Phase, J. Phys. Chem. Ref. Data 14, no. 4, 947-970

671 Karion, A., C. Sweeney, P. Tans, T. Newberger (2010), AirCore: An innovative atmospheric
672 sampling system, J. Atmos. Oceanic Technology 27, 1839-1853. doi:
673 10.1175/2010JTECHA1448.1

674 Lekner, J. (2019), Laminar viscous flow through pipes, related to cross-sectional area and
675 perimeter length, Am. J. Phys. 87, 791, doi: 10.1119/1.5113573

676 Massman, W. (1998), A review of the molecular diffusivities of H_2O, CO_2, CH_4, CO, O_3, NH_3,
677 N_2O, NO, and NO_2 in air, O_2 and N_2 near STP, Atmos. Environm. 32, 1111-1127

678 Membrive, O., C. Crevoisier, C. Sweeney, F. Danis, A. Hertzog, A. Engel, H. Bönish, and L.
679 Picon (2017), AirCore-HR: a high resolution column sampling to enhance the vertical
680 description of CH_4 and CO_2, Atmos. Meas. Tech. 10, 2163-2181, doi: 10.5194/amt-10-2163-
681 2017

682 Moore, F., E. Ray, K.Rosenlof, J. Elkins, P.Tans, and C.Sweeney (2014), A cost effective trace
683 gas measurement program for long term monitoring of the stratospheric circulation, Bull. Amer.
684 Meteo. Soc., 95, 147-155, doi: 10.1175/BAMS-D-12-00153.11G

685 O'Hanlon, J. (1980), A user's guide to vacuum technology, Wiley & Sons, New York, ISBN 0-
686 471-01624-1

687 Press, W., S. Teukolski, W. Vetterling, and B. Flannery (1992), Numerical Recipes in Fortran,
688 2nd Edition, Cambridge University Press, ISBN 0-521-43064-X

689 Sevast'yanov, R., and R. Chernyavskaya (1986), Virial coefficients of nitrogen, oxygen, and air
690 at temperatures from 75 to 2500 K, J. Engineer., Phys. and Thermophys. 51, 851-854.

691 Swagelok (2020), Valve Sizing Technical Bulletin, downloaded September 2020 from
692 www.swagelok.com/en/toolbox/cv-calculator

693 Tans, P. (2009), System and method for providing vertical profile measurements of atmospheric
694 gases. U.S. Patent 7,597,014 (6 Oct. 2009)

695 VIM3, International vocabulary of metrology – Basic and general concepts and associated terms,
696 JCGM 200:2008, published by Bureau International de Poids et Mesures (BIPM).

697 Wagenhäuser, T., A. Engel, R. Sitals (2021), Testing the altitude attribution and vertical
698 resolution of AirCore measurements with a new spiking method, Atmos. Meas. Techn. 14, 1-12,
699 doi: 10.5194/amt-14-1-2021.

700